CHEMISTRY OF MATERIALS

pubs.acs.org/cm

Article

Integration of Fluorescent Functionality into Pressure-Amplifying Metal–Organic Frameworks

Francesco Walenszus, Jack D. Evans, Volodymyr Bon, Friedrich Schwotzer, Irena Senkovska, and Stefan Kaskel*

Cite This: *Chem. Mater.* 2021, 33, 7964–7971

Read Online

ACCESS | Metrics & More | Article Recommendations | Supporting Information

ABSTRACT: The flexibility of soft porous crystals, i.e., their ability to respond to external stimuli with structural changes, is one of the most fascinating features of metal–organic frameworks (MOFs). In addition to breathing and swelling phenomena of flexible MOFs, negative gas adsorption (NGA) and pressure amplification (PA) are the more recent discoveries in this field initially observed in the cubic DUT-49 framework. In recent years, the structural contraction was monitored by physisorption, X-ray diffraction, nuclear magnetic resonance (NMR), and electron paramagnetic resonance (EPR) techniques, providing only limited information about the electronic structure of the ligand. In this work, we designed a new ligand with a fluorescent core in the linker backbone and synthesized three new MOFs, isoreticular to DUT-49, denoted as DUT-140(M) (M-Cu, Co, Zn), crystallizing in the space group $Fm\bar{3}m$. DUT-140(Cu) can be desolvated and is highly porous with an accessible apparent surface area of 4870 $m^2\ g^{-1}$ and a pore volume of 2.59 $cm^3\ g^{-1}$. Furthermore, it shows flexibility and NGA upon adsorption of subcritical gases. DUT-140(Zn), synthesized using postsynthetic metal exchange, could only be studied with guests in the pores. In addition to the investigation of the adsorption behavior of DUT-140(Cu), spectroscopic and computational methods were used to study the light absorption properties.

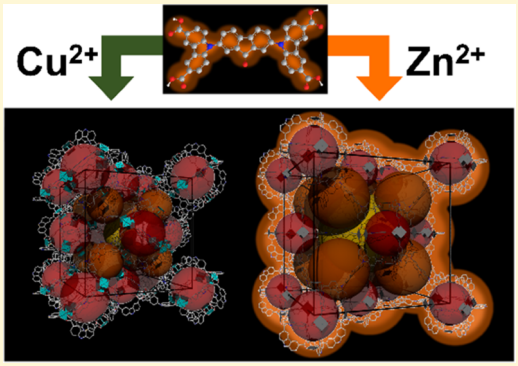

INTRODUCTION

Over the last two decades, metal–organic frameworks (MOFs) have been established as a new class of highly porous coordination networks consisting of inorganic nodes (metal ions or metal-oxo clusters) and linker molecules. In this context, linkers are defined as polydentate organic ligands, which interconnect the inorganic nodes.[1−4] MOFs contain voids accessible to various probe molecules that can be used for many applications.[5] Due to this modular design, there are almost no limits regarding structural nodes combination, resulting in a wide variety of frameworks with different topologies. In addition to excellent tunability of the material properties, MOFs often show immense surface areas[6,7] with permanent porosity. A limited number of MOFs also show structural flexibility, reflected in a distinct structural response to external stimuli, which can be considered among the most unique and fascinating properties compared to traditional porous solids. The phenomenon was first predicted in 1998[8] as an attribute of the third generation of MOFs, which are also known as flexible MOFs or soft porous crystals.[2] The dynamic behavior of soft porous crystals could be exploited in the last decades in a range of different applications like gas separation,[9−11] molecular sensing,[12−14] drug delivery,[15,16] and improved storage and release of gases,[17] outperforming the rigid analogues. Different types of flexibility phenomena such as breathing, swelling, and subnetwork displacement have been described,[6,18] reflected in very specific adsorption characteristics and isotherm shapes.[19]

In 2016, a previously unknown phenomenon, later denoted as negative gas adsorption (NGA), was discovered in the metal–organic framework DUT-49, reflected by spontaneous gas desorption and pressure amplification (PA) upon breathing. DUT-49 is built from the tetratopic 9,9′-([1,1′-biphenyl]-4,4′-diyl)-bis(9*H*-carbazole-3,6-dicarboxylate) (BBCDC) ligand and copper paddle-wheel units. From a structural point of view, the material consists of cuboctahedral metal–organic polyhedra (MOP) formed by copper paddle wheels and 3,6-carbazole-dicarboxylates, which are interconnected by 4,4′-biphenyl units forming close cubic packing. This linkage generates a hierarchical pore system of cuboctahedral (10 Å), tetrahedral (17 Å), and octahedral (24 Å) pores. During adsorption of subcritical gases at conditions close to the standard boiling point, the network shows a transition to a

Received: May 27, 2021
Revised: September 6, 2021
Published: October 6, 2021

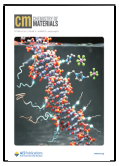

https://doi.org/10.1021/acs.chemmater.1c01804
Chem. Mater. 2021, 33, 7964–7971

contracted pore (cp) phase, while previously adsorbed gas is expelled, leading to a pressure amplification (PA) in the measurement cell. This transformation is different from other materials, uniquely caused by a switch-like, out-of-plane buckling of the sp^2-hybridized biphenyl part of the BBCDC linker.[20,21] Molecular simulations have highlighted the origin of the contraction during methane adsorption,[22] and in later work also, the effects of crystallite size[23] and pore size in an isoreticular series[24] on the mechanical properties and the transition were investigated. Recent research on this material enlightens the switching behavior and the effect of defects using nuclear magnetic resonance (NMR) techniques.[25,26] Furthermore the impact of temperature and choice of adsorbate on the NGA step was examined in more detail.[27,28] Today, pressure amplification by NGA can approach higher pressures beyond 400 kPa, which may be valuable for pneumatic applications.[29]

The guest-dependent flexibility of DUT-49 was extensively investigated by *in situ* X-ray diffraction/adsorption experiments, computational methods,[20,22−24] and *in situ* NMR experiments.[25,26,30] However, none of these techniques address the changes in electronic states of the ligand molecule in detail. This aspect can be tackled by optical spectroscopic techniques and would give a deeper insight into changes in the electronic and molecular structure of the linker in response to the contraction trajectory. Further investigation of the linker in the closed pore phase allows consideration of the question if the contraction of the network can be used to arrest a fragment of the linker in unnatural conformational states. This can not only be interesting for uncommon fluorescence properties but also for an activation of reactive centers by increasing the accessibility, for example.

In 2002, fluorescence was mentioned for the first time in connection with MOFs.[31] Since then, different strategies were used to integrate fluorescent moieties into MOFs especially for sensing applications.[32,33] For instance, it was found that the stiffening of luminophores in networks increases their fluorescence intensity because of decreased vibrational decay. Furthermore, the precise spatial fixation of fluorophores within a lattice can significantly influence the fluorescence properties and lead to interesting effects like J dimer emission[34] or multiemission.[35,36] Also, phenomena like charge and energy transfer, known from classical coordination chemistry, were observed.[31,37] In addition to pure ligand-based fluorescence, MOFs containing d^{10} ions often exhibit metal-to-ligand (MLCT) and ligand-to-metal charge transfer (LMCT).[31] Alternatively, fluorophores can be introduced into the pore system, which can lead to interesting emission properties.[36] Another possibility is offered by lanthanide-based MOFs where highly absorbing linker molecules are used to populate the emissive states of the lanthanide to increase its luminescence.[31,38,39]

In this work, a fluorescent probe was introduced into the DUT-49 framework. For this reason, the biphenyl moiety in the H_4BBCDC ligand of DUT-49 was exchanged by fluorenone, due to the structural similarity and, therefore, expected NGA behavior. To examine the possibility of NGA using 9,9′-(9-oxo-9*H*-fluorene-2,7-diyl)-bis(9*H*-carbazole-3,6-dicarboxylic acid) (H_4FBCDC) as a linker, a computational study on the mechanical properties of the ligand was conducted and compared with the H_4BBCDC ligand. Subsequently, the fluorenone-based ligand was synthesized and incorporated into DUT-140(Cu), a MOF isoreticular to DUT-49. The adsorption properties of DUT-140(Cu) were investigated and the NGA behavior was observed upon adsorption of methane at 111 K. To enable the fluorescence detection and to avoid paramagnetic fluorescence quenching, DUT-140(Zn) was synthesized by postsynthetic metal exchange. The influence of the mechanical stress and linker deformation on fluorescence properties was further investigated in desolvation experiments.

EXPERIMENTAL SECTION

Synthesis of Microcrystalline MOF Powders. The microcrystalline powder of metal−organic framework DUT-140(Cu) was synthesized by a solvothermal approach. In a 500 mL round bottom flask, the H_4FBCDC ligand (500 mg, 7.73 mmol, 1.00 equiv) was dissolved in 200 mL of *N*,*N*-dimethylformamide (DMF) under inert atmosphere and 20 mL of acetic acid was added. Sometimes, a part of the ligand precipitates again after addition of acetic acid. Careful heating of the mixture up to 80 °C supports the solution procedure in this case. Subsequently, $Cu(NO_3)_2(H_2O)_{2.5}$ (423 mg, 1.82 mmol, 2.50 equiv) was added and the reaction mixture was stirred for 72 h at 80 °C while fine green powder precipitated. After the reaction, the obtained powder was washed five times with DMF. A small amount of the washed precipitate was used for powder X-ray diffraction (PXRD) measurements, referred to as the "as-made" MOF. Desolvation of DUT-140(Cu) was achieved using a supercritical point dryer and resulted in 212 mg (36%) of pure and highly crystalline MOF powder.

DUT-140(Co) was synthesized using the same procedure as for the copper analogue. H_4FBCDC linker (200 mg, 0.29 mmol, 1.00 equiv) was dissolved in 75 mL of *N*-methyl-2-pyrrolidone (NMP). To this, a solution of cobalt nitrate hexahydrate (212 mg, 0.73 mmol, 2.50 equiv) was added and the resulting mixture was stirred for 72 h at 80 °C under inert atmosphere until a brownish precipitate was formed. After completion of the reaction, the crystals were washed three times with pure NMP. A part of the product was separated for PXRD analysis.

DUT-140(Zn) was obtained by postsynthetic metal exchange from DUT-140(Co). Therefore, the solvent above the washed DUT-140(Co) crystals was exchanged by a 0.1 M solution of $Zn(NO_3)_2(H_2O)_6$. The supernatant solution was renewed six times over 2 days. During the first three exchange steps, the supernatant solution turned violet. After the color completely faded, the zinc nitrate solution was refreshed three more times and the product was subsequently washed three times with NMP.

***In Situ* Fluorescence Measurements upon Desolvation.** The *in situ* desolvation experiment was performed in a solid-state sample holder filled with the solvated material in acetone. The sample holder was positioned at 45° between the incident beam and the detector. The solvent was evaporated over 25 h and fluorescence spectra were measured every 5 min.

***In Situ* PXRD upon Desolvation.** The powder of DUT-140(Zn) in ethanol was prepared using a background-free holder for measurements under inert conditions and covered by 7.5 μm thick Kapton foil to ensure a slow solvent evaporation. The measurements were performed on an Empyrean 2 diffractometer (Panalytical) using Cu Kα1 irradiation and Pixcel3D detector. A total of 173 measurements were performed in the 2θ range of 7−10° with exposition time of 100 s for each measurement.

RESULTS AND DISCUSSION

***In Silico* Investigations of DUT-140.** The breathing mechanism responsible for NGA in DUT-49 is related to a deformation of the BBCDC linker, further denoted as ligand buckling.[22] In previous works, a method was developed to allow an investigation of the mechanical properties of ligands, which directly reflect the switchability and the probability of NGA in frameworks isoreticular to DUT-49.[20,24] This was achieved by calculating stress−strain curves for the single

https://doi.org/10.1021/acs.chemmater.1c01804
Chem. Mater. 2021, 33, 7964−7971

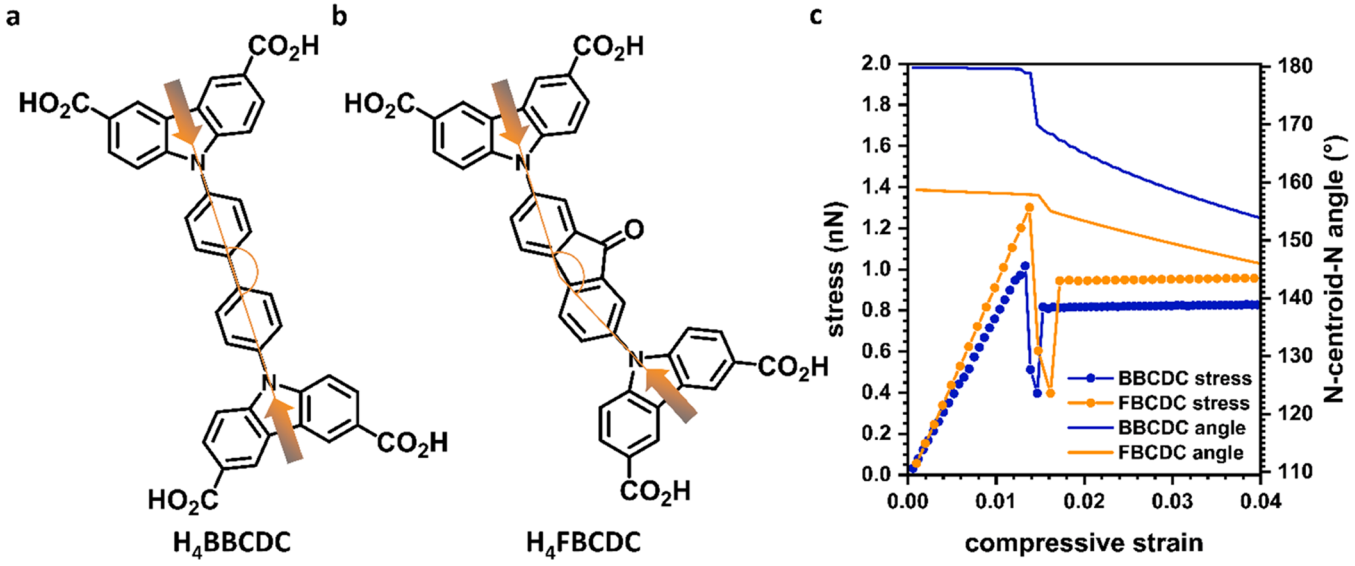

Figure 1. (a) H_4BBCDC and (b) H_4FBCDC linker molecules. (c) Stress−strain curve of the ligands (dotted line). The direction of the applied pressure is indicated by the orange arrows. Evolution of N−centroid−N angle of the ligands (solid line) while strain is applied.

ligand using density functional theory (DFT) methods. Therefore, simulations were performed also for the H_4FBCDC ligand before synthetic efforts were made.

The mechanical properties of H_4FBCDC were determined by simulated compression of the linker at the carbazole nitrogens (orange arrows, Figure 1a,b) using the accurate tight-binding quantum chemical method GFN2_xtb.[40] From these calculations, stress applied to the ligand can be determined and the mechanical stability in addition to the response of network-induced pressure can be explored as shown for H_4BBCDC (blue) and H_4FBCDC (orange) in Figure 1c. Initially, increasing the compressive strain to both linkers results in an elastic response up to a certain point, defining the maximal stress. After reaching this point, the ligand itself starts to buckle (Figure 2). This step in the stress−strain curve is a common feature of all ligands used for the synthesis of NGA materials.[24] As derived from the graph in Figure 1c, maximum stress for each linker is reached at ∼0.014 compressive strain. The H_4FBCDC ligand reaches the maximum yield stress at 1.30 nN, which is higher compared to that of H_4BBCDC that demonstrates an inelastic transition at 1.02 nN. Furthermore, Young's modulus, reflected by the linear slope of the stress−strain curve, is also larger for H_4FBCDC. The demonstrated strain resistance behavior shows that the intended linker is more rigid than the DUT-49 linker, which follows chemical intuition based on comparison of the chemical structures.

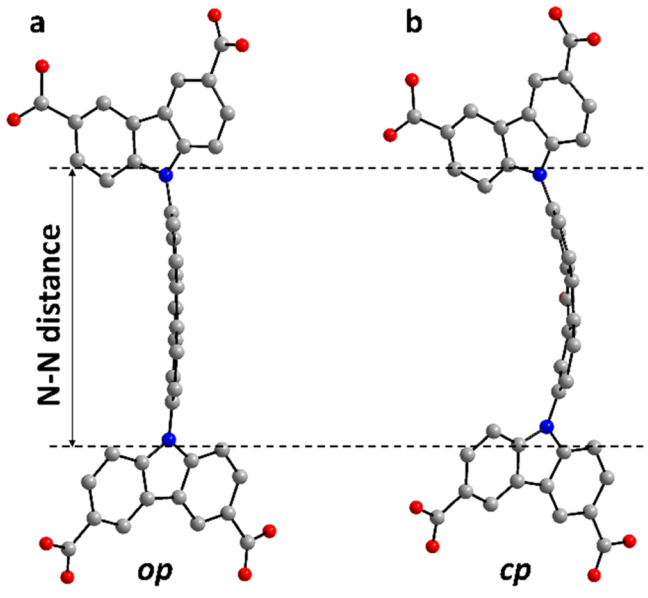

Figure 2. Deflection of the H_4FBCDC ligand at (a) 0.00 nN and (b) 0.03 nN compressive strain. color code: gray: carbon, blue: nitrogen, red: oxygen. Hydrogen atoms are omitted for clarity.

These simulations also demonstrate that the overall deflection for H_4BBCDC is larger than that for H_4FBCDC. The pore sizes of the related op phases of corresponding MOFs do not differ significantly, as shown in Supporting Information Figure S8. The performance of an NGA material cannot be directly derived from the stress−strain curve; however, the increased rigidity of H_4FBCDC is expected to permit an overloading of the metastable state, increasing the NGA step. However, increased rigidity may also lead to a reduction of the ligand deflection, which in turn could lead to a hindered contraction.

Experimental Investigation of Desolvated DUT-140(Cu). As the theoretical calculations of the mechanical properties of H_4FBCDC predict the potential for NGA, the ligand was synthesized in a similar six-step approach used for the synthesis of recently reported elongated versions of H_4BBCDC.[24] The carbazole was converted to dibutyl-9*H*-carbazole-dicarboxylate over four steps and the obtained dicarboxylate was used as the starting material in an Ullman-coupling reaction with 2,7-dibromofluorenone. After the subsequent hydrolysis and purification, the H_4FBCDC ligand was obtained in 28% yield over six steps. All compounds have been analyzed by ^{1}H and ^{13}C NMR as well as by mass spectroscopy and IR spectroscopy as shown in Supporting Information chapter 2.

The reaction of H_4FBCDC with copper(II)nitrate in *N*,*N*-dimethylformamide (DMF) yields the framework with a composition $[Cu_2(FBCDC)](H_2O)_x(DMF)_y$, denoted as

https://doi.org/10.1021/acs.chemmater.1c01804
Chem. Mater. 2021, 33, 7964−7971

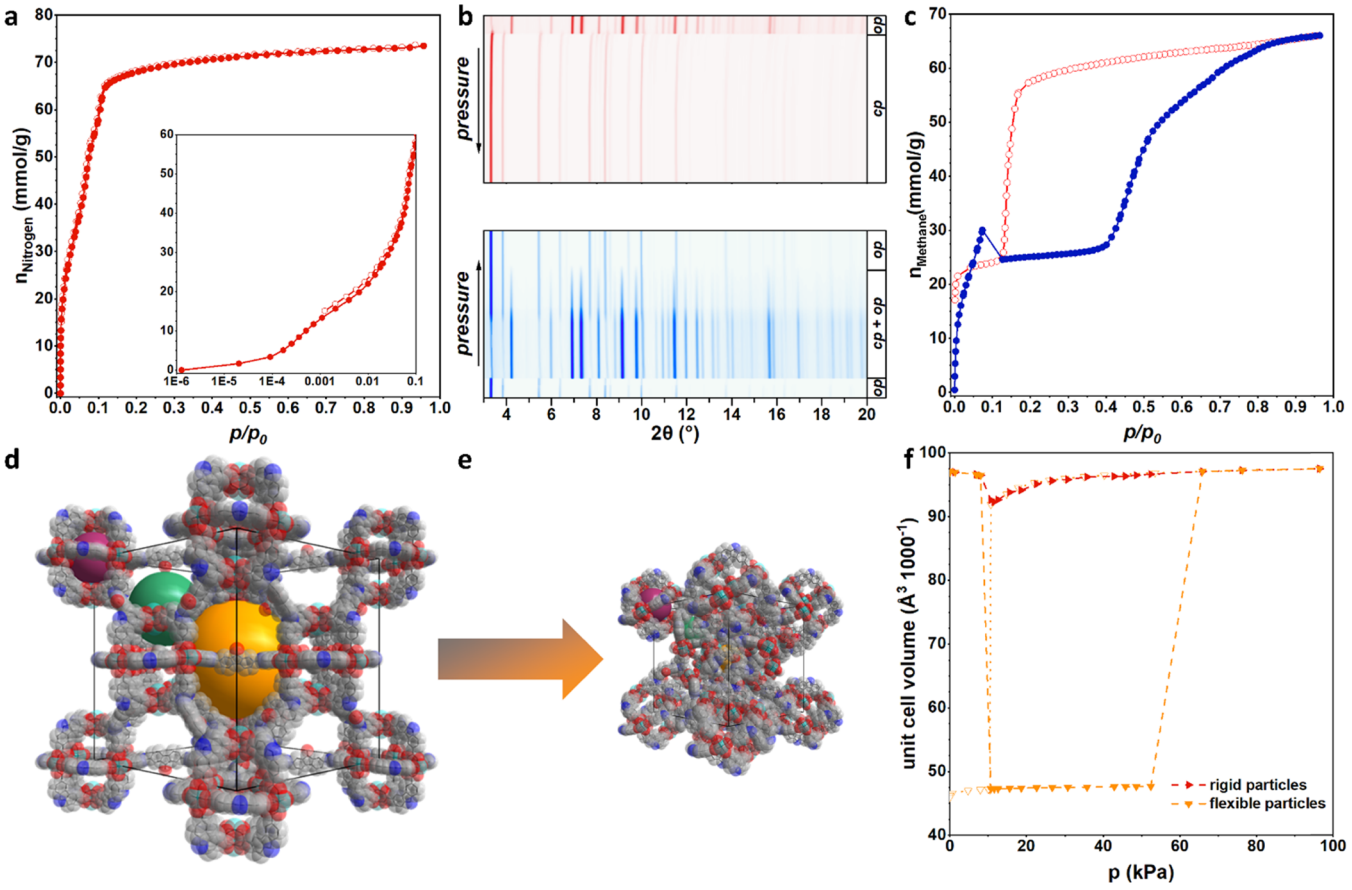

Figure 3. Crystal structure and adsorption-induced switching in DUT-140(Cu). (a) Physisorption of nitrogen on DUT-140(Cu) at 77 K (inset shows the low-pressure range in semilogarithmic scale). (b, c) *In situ* PXRD patterns and the corresponding physisorption isotherm measured upon adsorption (blue) and desorption (red) of methane at 111 K. (d) Crystal structure of the op phase of DUT-140(Cu). (e) Crystal structure of the cp phase of DUT-140(Cu). Voids are shown as colored spheres (purple: cuboctahedral, green: tetrahedral, and orange: octahedral cavities). (f) Evolution of the unit cell volume upon adsorption (filled triangles) and desorption (open triangles) of methane on DUT-140(Cu) at 111 K (red triangles: rigid and orange triangles: flexible crystallites).

DUT-140(Cu). The MOF was synthesized using two different synthesis routes yielding crystalline powders with an average particle size of 14 μm and single-crystal sample with crystals up to 100 μm (Supporting Information chapters 3.1 and 3.3.5). The crystal structure of the DUT-140(Cu) was determined by means of synchrotron single-crystal X-ray diffraction at MX BL14.3 beamline of the BESSY-II light source. DUT-140(Cu) crystallizes in the cubic space group $Fm\bar{3}m$ (No. 225) with lattice parameter a = 46.14 Å and is isostructural to DUT-49 (Supporting Information, chapter 3.3.2). Detailed analysis of the ligand molecule in the crystal structure shows elongated thermal ellipsoids even for the carbazole moiety, indicating disorder that can be caused by vibration of the molecule in the direction perpendicular to the carbazole plane. Since the symmetry of the fluorenone backbone is lower than the symmetry of the corresponding position in the space group, the fluorenone moiety is disordered over four positions.

The material has a hierarchical pore system with three different voids (11, 16, 24 Å). The phase purity of DUT-140(Cu) was confirmed by PXRD (Supporting Information chapter 3.3). The activated powder sample of DUT-140(Cu) was subjected to physisorption experiments using nitrogen at 77 K and methane at 111 K as probe molecules (Figure 3a,c). The low-pressure range of the nitrogen isotherm, shown in Figure 3a, displays superimposing steps up to p/p_0 = 0.1, indicating the consecutive filling of the pores before reaching saturation. The desorption branch shows no hysteresis and therefore no indications of the structural flexibility. The isotherm reaches saturation at 73.5 mmol/g, which is slightly lower than the theoretically calculated capacity of 74.6 mmol/g. The shape of the methane adsorption isotherm at 111 K (Figure 3c) is similar to the methane isotherm for DUT-49 at the same temperature. In the low-pressure range, the stepwise pore filling occurs up to p/p_0 = 0.075, at which the NGA event is observed with Δn_{NGA} = 5.45 mmol/g. The second step is observed at relative pressures between 0.4 and 0.6 and is associated with the structure reopening in the case of DUT-49. The isotherm reaches the second plateau at p/p_0 = 0.8 with a resulting adsorption capacity of 63.4 mmol/g. The desorption branch of the isotherm is characterized by a plateau at p/p_0 = 0.9−0.1, which is followed by the steep desorption step and the second plateau at p/p_0 < 0.1. The intersection range of adsorption and desorption branches indicates the metastability range for the structure (Figure 3c). To monitor the structural transitions upon adsorption of methane at 111 K, the same experiment was reproduced in the external adsorption cell, inserted in the synchrotron beam of KMC-2 beamline (BESSY-II). The PXRD patterns collected are shown as profile contour plots in Figure 3b. PXRD patterns confirm structural contraction from the op to cp phase upon NGA

https://doi.org/10.1021/acs.chemmater.1c01804
Chem. Mater. 2021, 33, 7964−7971

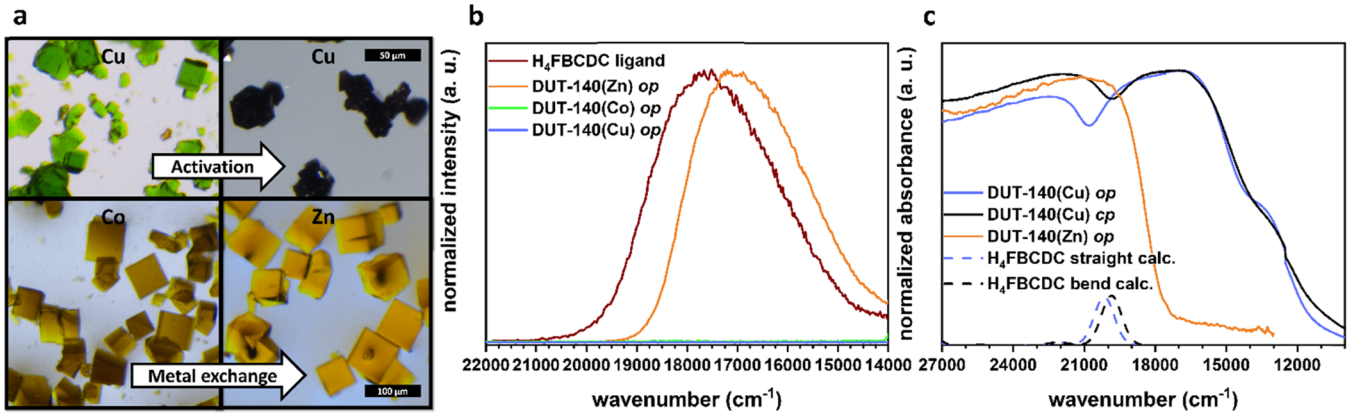

Figure 4. (a) Microscopic images of DUT-140(M) crystals, top line: DUT-140(Cu) before and after activation, bottom line: DUT-140(Co) after synthesis and DUT-140(Zn) after metal exchange. (b) Fluorescence spectra of dissolved fluorenone ligand (3 mM) and DUT-140(M)_op suspended in NMP. Excitation wavelength: 365 nm. (c) Absorption spectra of DUT-140(Cu) op and cp phases and DUT-140(Zn)_op. Dotted lines correspond to a specific excitation in the stretched (blue) and contracted (black) form of H_4FBCDC.

event, showing a shift of (111) reflection toward higher 2θ angle, similar to that observed for DUT-49. In the relative pressure range of 0.1−0.5, a mixture of the op and cp phases is observed that can be explained by broad crystallite size distribution, a phenomenon known for DUT-49.[23]

Detailed analysis of the crystal size distribution (Supporting Information Figure S6) shows a distinct number of crystallites smaller than 1 μm, which was defined as a critical particle size for structural transition in DUT-49 during adsorption of nitrogen at 77 K. However, since DUT-140(Cu) shows higher resistance to the adsorption stress, the particle size dependency could be transferred to the adsorption of methane at 111 K. The second step in the adsorption branch is characterized by the structural reopening. Interestingly, during the desorption no intermediate (ip) phases were observed, as it is known for DUT-49.[20] After complete desorption of methane at 111 K, DUT-140 stays in the cp phase. The monitoring of the cell volume also points out that even the rigid part of the sample, namely, the smaller crystals, shows a slight response to the stress associated with the adsorption of methane (Figure 3f).

Fluorescence in DUT-140(Cu). Photoluminescence properties of the H_4FBCDC ligand in solution and within the suspended metal−organic framework in the solid state were investigated at room temperature. According to the fluorescence spectra (Figure 4b), a 3 mM solution of H_4FBCDC ligand in NMP shows a yellow emission with a maximum at 17 750 cm^{-1} ($\lambda_{Ext.}$ = 27 397 cm^{-1}). However, no fluorescence of the solid linker powder can be observed. This fluorescence quenching in the solid state is most likely due to the efficient $\pi-\pi$-stacking of the ligands. In contrast, in the crystal of DUT-140, the MOPs are interconnected by the fluorenone-containing backbones into a three-dimensional structure. As a result, the fluorenone moieties are isolated from other groups and therefore not involved in any weak interaction, which prevents fluorescence quenching as shown in Figure S10 of the Supporting Information. However, d−d transitions in the d^9 Cu^{2+} ions still hinder an investigation of the fluorescence in the framework. As a result, no fluorescence can be detected after crystallization of the MOF, as this is suppressed due to the complex formation and quenching.

Nevertheless, the UV/vis spectra of the DUT-140(Cu) in the op and cp phases were recorded and compared with simulated UV/vis spectra of the straight and bent ligands (Figure 4c). DUT-140(Cu) shows strong absorption in the range of 15 000−27 500 cm^{-1}. This absorption is divided by a small local minimum whereby the absorption band at higher wavenumbers can be attributed to the linker absorption and the absorption band at lower wavenumbers originates from the metal centers.

The contraction of DUT-140(Cu) from the op (blue line) to the cp (black line) phase causes a red shift of the first absorption maximum. The simulated absorption spectra of the linker in the stretched and bent forms (Figure 4c dotted lines) show the same trend for the shift in absorbance for a $\pi-\pi^*$ excitation from carbazoles to the fluorenone system (Figure S11) at around 20 000 cm^{-1}. This observation indicates changes in the electronic structure of the linker during contraction and an excitation at lower energies for the cp phase of the network.

Metal Exchange. To detect the fluorescence of the metal−organic framework, it is necessary to replace copper by a spectroscopically "silent" metal, which is similarly capable of forming paddle-wheel units. Regarding these requirements, Zn^{2+} is a suitable target metal because of d^{10} electronic configuration. However, direct synthesis of DUT-140(Zn) starting from the ligand and zinc salt was not successful.

Therefore, the metal exchange approach, recently reported by our group for DUT-49,[41] was used and first attempts were made to synthesize cobalt-based DUT-140 using NMP as a solvent. The obtained single crystals were repeatedly washed with fresh NMP and afterward the brownish DUT-140(Co) crystals were exposed to 0.1 M zinc nitrate solution in NMP. The change of the crystal color from initial brown to distinct orange with simultaneous violet coloration of the supernatant solution indicates the metal exchange. To confirm the complete metal exchange, energy-dispersive X-ray (EDX) measurements were conducted as shown in Figure S7. Figure 4a shows the color evolution of the crystals during the metal exchange procedure. Furthermore, it can be clearly seen that the cubic morphology of the crystals remains after the metal exchange. Single-crystal X-ray diffraction experiments reveal that DUT-140(Co) and DUT-140(Zn) are isostructural to DUT-140(Cu). The crystal structures of both materials were solved in the space group $Fm\bar{3}m$ (No. 225) with lattice parameters a = 46.47 Å for DUT-140(Co) and a = 46.52 Å for DUT-140(Zn) (Supporting Information, chapter 3.3.2). The

https://doi.org/10.1021/acs.chemmater.1c01804
Chem. Mater. 2021, 33, 7964−7971

crystal structures confirm the trend for the M−M distance within the paddle wheel, previously observed in the DUT-49(M) frameworks and dictated by Irving−Williams series showing the M−M distance in the series: 2.6314(10) Å in DUT-140(Cu), 2.8335(15) Å in DUT-140(Co), and 2.9917(10) Å in DUT-140(Zn).[41] The increased M−M distance in DUT-140(Co) and DUT-140(Zn) leads to lower thermodynamic stability of the corresponding paddle wheels and as a consequence, amorphization of the frameworks upon supercritical CO_2 drying procedure as shown in Supporting Information chapter 3.3.1. Nitrogen physisorption at 77 K on DUT-140(Co) (Supporting Information chapter 3.3.8) reveals neglectable capacity compared to DUT-140(Cu), leading to the conclusion of structural collapse upon supercritical activation.

In addition to the synthesis of a new responsive MOF and the successful metal replacement, the initial goal was finally achieved by this procedure as shown in Figure 4b. In addition to DUT-140(Cu) (blue line) and DUT-140(Co) (green line), which are both nonluminescent, the fluorescence properties of the linker in DUT-140(Zn) (orange line) were observed.

Fluorescence in DUT-140(Zn). In comparison with the ligand, the spectrum of DUT-140(Zn) shows a red-shifted emission maximum at 17 000 cm^{-1}. This behavior is attributed to coordination to the metal center. Since suspended crystals were used to record fluorescence spectra, a comparison of luminescence intensity with that of the dissolved linker is not feasible.

Unfortunately, the desolvation of the DUT-140(Zn) framework even using supercritical CO_2 drying leads to amorphization of the material. Therefore, studies on the guest-free DUT-140(Zn) are not possible at this stage and the following experiments were performed on solvated crystals.

Time-resolved Desolvation Experiment. Garai et al. demonstrated a structural transition from the op to intermediate (ip) phase taking place upon solvent desorption in case of DUT-49(Zn), identified by time-resolved *in situ* PXRD.[42] Therefore, we conducted two experiments to investigate the effect of desolvation on the fluorescence properties of DUT-140(Zn). At first, the solvent in the pores of as-made DUT-140(Zn) was replaced by acetone. In an *in situ* experiment, the evaporation of acetone was followed by fluorescence spectroscopy.

Figure 5a shows the fluorescence decay during desolvation from acetone. The spectra show two main features: a decrease in fluorescence intensity during desolvation and second, a slight red shift of the fluorescence maximum from about 17 000 cm^{-1} to about 16 500 cm^{-1}. Accordingly, there is a change in the fluorescence properties during the desolvation of the material. To examine whether this change is related to a structural change of the material, an *in situ* PXRD experiment was performed. The contour plot in Figure 5b does not show a shift of the individual reflections with time. Therefore, no structural contraction to another crystalline phase can be assumed for DUT-140(Zn) compared to DUT-49(Zn), showing the transition from the op to ip phase upon solvent desorption before amorphization.[42]

Although all previous experiments clearly indicate that there might be a change in fluorescence due to the structural change of the material, no evidence for this hypothesis can be found from these experiments and the red shift can be attributed to the amorphization and rupture of some coordination bonds.

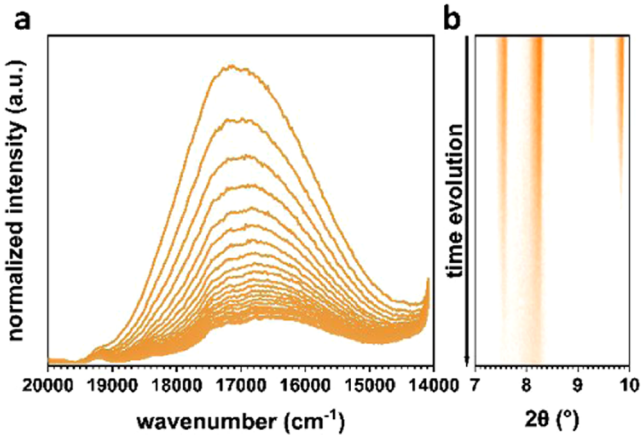

Figure 5. Time-dependent desolvation experiments on DUT-140(Zn). (a) Fluorescence decay over desolvation from acetone. Spectra are recorded every 5 min for 25 h. (b) In situ PXRD over desolvation from EtOH. PXRD was recorded every 115 s over 5.5 h.

This behavior is most likely caused by the fine interplay of the lower stability of the zinc paddle-wheel unit compared to the copper paddle-wheel unit and the higher rigidity of the H_4FBCDC ligand (DUT-140) compared to the H_4BBCDC ligand (DUT-49). The more rigid H_4FBCDC linker does not even allow a small contraction of the network due to desorption stress and capillary forces before the coordination bond within the zinc paddle-wheel breaks. For DUT-49(Zn) in comparison, the difference between the paddle-wheel stability and the linker rigidity is small enough for a contraction to intermediate phase before the coordination bond breaks.

This finding leads to the assumption that a linker with smaller rigidity than that of DUT-49 linker could lead to a network that shows a full contraction before amorphization during solvent evaporation.

CONCLUSIONS

In brief, three new MOF materials DUT-140(M) (M = Cu, Co, Zn) were successfully synthesized. As predicted by mechanical considerations of the H_4FBCDC ligand, the metal−organic framework DUT-140(Cu) shows intrinsic flexibility as well as a negative gas adsorption property with Δn_{NGA} = 5.45 mmol/g. The contraction of the op phase can be induced by adsorption of methane at 111 K. Adsorption experiments also confirm the assumption that the use of the H_4FBCDC linker leads to a more rigid network since the adsorption of nitrogen does not trigger the phase transformation.

UV/vis investigations of DUT-140(Cu) showed a distinct change in the absorption spectrum, which is in line with DFT calculations and could be attributed to an excitation from the carbazole moiety to the fluorenone part. Since this excitation is strongly affected by the deformation of the linker, it can be concluded that the fluorescence spectrum also should change under the given conditions due to the structural transformation.

The fluorescence properties of the MOF could be unveiled by an exchange of the metal node to a zinc paddle wheel. However, the stiffening of the metal−organic framework did not lead to the desired increased resistance to desolvation stress for DUT-140(Zn), indicating the metal node to be the main limiting factor, leading to amorphization during desol-

https://doi.org/10.1021/acs.chemmater.1c01804
Chem. Mater. 2021, 33, 7964−7971

vation in such highly porous framework materials, even under mild supercritical conditions.

In situ fluorescence studies provide clear evidence that a fluorescence change is caused by structural decomposition of the metal−organic framework and reveal the importance of the fine interplay of linker rigidity and metal node stability for the investigation of structural contraction by solvent desorption.

Overall, fluorenone moieties are valuable functional building blocks for the detection of structural dynamics in the organic sublattice of porous framework compounds.

■ ASSOCIATED CONTENT

Supporting Information

The Supporting Information is available free of charge at https://pubs.acs.org/doi/10.1021/acs.chemmater.1c01804.

Synthesis and characterization of organic compounds, PXRD, SEM, EDX, and TGA (PDF)

Crystallographic data for DUT-140(Cu), DUT-140(Zn), and DUT-140(Co) (CCDC-2080449-2080451) can be obtained free of charge from the Cambridge Crystallographic Data Centre via www.ccdc.cam.ac.uk/data_request/cif (CIF)

Adsorption for nitrogen (77K) (TXT)

Adsorption for methane (111 K) (TXT)

■ AUTHOR INFORMATION

Corresponding Author

Stefan Kaskel − *Anorganische Chemie I, Fakultät Chemie und Lebensmittelchemie, Technische Universität Dresden, 01062 Dresden, Germany;* orcid.org/0000-0003-4572-0303; Email: stefan.kaskel@tu-dresden.de

Authors

Francesco Walenszus − *Anorganische Chemie I, Fakultät Chemie und Lebensmittelchemie, Technische Universität Dresden, 01062 Dresden, Germany*

Jack D. Evans − *Anorganische Chemie I, Fakultät Chemie und Lebensmittelchemie, Technische Universität Dresden, 01062 Dresden, Germany;* orcid.org/0000-0001-9521-2601

Volodymyr Bon − *Anorganische Chemie I, Fakultät Chemie und Lebensmittelchemie, Technische Universität Dresden, 01062 Dresden, Germany;* orcid.org/0000-0002-9851-5031

Friedrich Schwotzer − *Anorganische Chemie I, Fakultät Chemie und Lebensmittelchemie, Technische Universität Dresden, 01062 Dresden, Germany*

Irena Senkovska − *Anorganische Chemie I, Fakultät Chemie und Lebensmittelchemie, Technische Universität Dresden, 01062 Dresden, Germany;* orcid.org/0000-0001-7052-1029

Complete contact information is available at: https://pubs.acs.org/10.1021/acs.chemmater.1c01804

Author Contributions

F.W. synthesized, activated, and performed characterization of organic ligands and MOF samples. F.W. and V.B. contributed to *in situ* PXRD measurements. V.B. performed refinement of PXRD data. F.W., V.B., J.D.E., I.S., and S.K. contributed to analysis, interpretation, and discussion of adsorption and single-crystal X-ray diffraction data. J.D.E. performed computational analysis of mechanical and adsorption properties. F.S. performed SEM and EDX analysis. F.W., V.B., J.D.E., I.S., and S.K. organized the project. All authors contributed to writing and improving the manuscript.

Funding

This project has received funding from the European Research Council (ERC) under the European Union's Horizon 2020 research and innovation program (grant agreement no. 742743), the BMBF (No. 05K19OD2), and ANR/DFG (Project Number 391704421).

Notes

The authors declare no competing financial interest.

■ ACKNOWLEDGMENTS

The authors thank the "Helmholtz-Zentrum Berlin für Materialien und Energie" for the allocated beamtime at KMC-2 (*in situ* PXRD) and D. Wallacher, D. M. Többens, and N. Grimm for support with the measurement setup, MX BL14.3 (single-crystal X-ray diffraction) beamlines of BESSY-II and travel funding. The authors thank Philipp Lange for performing elemental analysis. J.D.E. acknowledges the support of the Alexander von Humboldt Foundation and the Center for Information Services and High-Performance Computing (ZIH) at TU Dresden for providing high-performance computing facilities.

■ ABBREVIATIONS

DUT, Dresden University of Technology; MOF, metal−organic framework; MOP, metal−organic polyhedra; NGA, negative gas adsorption; op, open pore; cp, contracted pore; ip, intermediate pore; H_4BBCDC, 9,9′-([1,1′-biphenyl]-4,4′-diyl)-bis(9*H*-carbazole 3,6-dicarboxylic acid; H_4FBCDC, 9,9′-(9-oxo-9*H*-fluorene-2,7-diyl)-bis(9*H*-carbazole-3,6-dicarboxylic acid; MLCT, metal-to-ligand charge transfer; LMCT, ligand-to-metal charge transfer; DMF, *N*,*N*-dimethylformamide; NMP, 1-methylpyrrolidin-2-one; GCMC, Grand Canonical Monte Carlo

■ REFERENCES

(1) Batten, S. R.; Champness, N. R.; Chen, X.-M.; Garcia-Martinez, J.; Kitagawa, S.; Öhrström, L.; O'Keeffe, M.; Paik Suh, M.; Reedijk, J. Terminology of metal−organic frameworks and coordination polymers (IUPAC Recommendations 2013). *Pure Appl. Chem.* **2013**, *85*, 1715−1724.

(2) Horike, S.; Shimomura, S.; Kitagawa, S. Soft porous crystals. *Nat. Chem.* **2009**, *1*, 695−704.

(3) Furukawa, H.; Cordova, K. E.; O'Keeffe, M.; Yaghi, O. M. The Chemistry and Applications of Metal-Organic Frameworks. *Science* **2013**, *341*, No. 1230444.

(4) Zhou, H.-C.; Long, J. R.; Yaghi, O. M. Introduction to Metal−Organic Frameworks. *Chem. Rev.* **2012**, *112*, 673−674.

(5) Morris, R. E.; Wheatley, P. S. Gas Storage in Nanoporous Materials. *Angew. Chem., Int. Ed.* **2008**, *47*, 4966−4981.

(6) Bon, V.; Brunner, E.; Pöppl, A.; Kaskel, S. Unraveling Structure and Dynamics in Porous Frameworks via Advanced In Situ Characterization Techniques. *Adv. Funct. Mater.* **2020**, *30*, No. 1907847.

(7) Chen, Z.; Li, P.; Anderson, R.; Wang, X.; Zhang, X.; Robison, L.; Redfern, L. R.; Moribe, S.; Islamoglu, T.; Gómez-Gualdrón, D. A.; Yildirim, T.; Stoddart, J. F.; Farha, O. K. Balancing volumetric and gravimetric uptake in highly porous materials for clean energy. *Science* **2020**, *368*, 297−303.

(8) Kitagawa, S.; Kondo, M. Functional Micropore Chemistry of Crystalline Metal Complex-Assembled Compounds. *Bull. Chem. Soc. Jpn.* **1998**, *71*, 1739−1753.

(9) Liu, X.; Wang, M.; Zhou, S.; Wang, J.; Xin, H.; Wei, S.; Liu, S.; Wang, Z.; Lu, X. Tracking CO_2 capture and separation over N_2 in a

flexible metal−organic framework: insights from GCMC and DFT simulations. *J. Mater. Sci.* **2021**, *56*, 10414−10423.
(10) Sin, M.; Kavoosi, N.; Rauche, M.; Pallmann, J.; Paasch, S.; Senkovska, I.; Kaskel, S.; Brunner, E. In Situ ^{13}C NMR Spectroscopy Study of CO_2/CH_4 Mixture Adsorption by Metal-Organic Frameworks: Does Flexibility Influence Selectivity? *Langmuir* **2019**, *35*, 3162−3170.
(11) Dong, Q.; Zhang, X.; Liu, S.; Lin, R.-B.; Guo, Y.; Ma, Y.; Yonezu, A.; Krishna, R.; Liu, G.; Duan, J.; Matsuda, R.; Jin, W.; Chen, B. Tuning Gate-Opening of a Flexible Metal-Organic Framework for Ternary Gas Sieving Separation. *Angew. Chem., Int. Ed.* **2020**, *59*, 22756−22762.
(12) Freund, P.; Mielewczyk, L.; Rauche, M.; Senkovska, I.; Ehrling, S.; Brunner, E.; Kaskel, S. MIL-53(Al)/Carbon Films for CO_2-Sensing at High Pressure. *ACS Sustainable Chem. Eng.* **2019**, *7*, 4012−4018.
(13) Ingle, N.; Sayyad, P.; Deshmukh, M.; Bodkhe, G.; Mahadik, M.; Al-Gahouari, T.; Shirsat, S.; Shirsat, M. D. A chemiresistive gas sensor for sensitive detection of SO_2 employing Ni-MOF modified −OH-SWNTs and −OH-MWNTs. *Appl. Phys. A* **2021**, *127*, No. 157.
(14) Yang, Y.; Li, L.; Yang, H.; Sun, L. Five Lanthanide-Based Metal−Organic Frameworks Built from a π-Conjugated Ligand with Isophthalate Units Featuring Sensitive Fluorescent Sensing for DMF and Acetone Molecules. *Cryst. Growth Des.* **2021**, *21*, 2954−2961.
(15) Souza, B. E.; Donà, L.; Titov, K.; Bruzzese, P.; Zeng, Z.; Zhang, Y.; Babal, A. S.; Möslein, A. F.; Frogley, M. D.; Wolna, M.; Cinque, G.; Civalleri, B.; Tan, J.-C. Elucidating the Drug Release from Metal-Organic Framework Nanocomposites via In Situ Synchrotron Microspectroscopy and Theoretical Modeling. *ACS Appl. Mater. Interfaces* **2020**, *12*, 5147−5156.
(16) Suresh, K.; Matzger, A. J. Enhanced Drug Delivery by Dissolution of Amorphous Drug Encapsulated in a Water Unstable Metal-Organic Framework (MOF). *Angew. Chem., Int. Ed.* **2019**, *58*, 16790−16794.
(17) Sato, H.; Kosaka, W.; Matsuda, R.; Hori, A.; Hijikata, Y.; Belosludov, R. V.; Sakaki, S.; Takata, M.; Kitagawa, S. Self-Accelerating CO Sorption in a Soft Nanoporous Crystal. *Science* **2014**, *343*, 167−170.
(18) Aljammal, N.; Jabbour, C.; Chaemchuen, S.; Juzsakova, T.; Verpoort, F. Flexibility in Metal−Organic Frameworks: A Basic Understanding. *Catalysts* **2019**, *9*, 512.
(19) Schneemann, A.; Bon, V.; Schwedler, I.; Senkovska, I.; Kaskel, S.; Fischer, R. A. Flexible metal−organic frameworks. *Chem. Soc. Rev.* **2014**, *43*, 6062−6096.
(20) Krause, S.; Bon, V.; Senkovska, I.; Stoeck, U.; Wallacher, D.; Többens, D. M.; Zander, S.; Pillai, R. S.; Maurin, G.; Coudert, F.-X.; Kaskel, S. A pressure-amplifying framework material with negative gas adsorption transitions. *Nature* **2016**, *532*, 348−352.
(21) Stoeck, U.; Krause, S.; Bon, V.; Senkovska, I.; Kaskel, S. A highly porous metal−organic framework, constructed from a cuboctahedral super-molecular building block, with exceptionally high methane uptake. *Chem. Commun.* **2012**, *48*, 10841.
(22) Evans, J. D.; Bocquet, L.; Coudert, F.-X. Origins of Negative Gas Adsorption. *Chem* **2016**, *1*, 873−886.
(23) Krause, S.; Bon, V.; Senkovska, I.; Többens, D. M.; Wallacher, D.; Pillai, R. S.; Maurin, G.; Kaskel, S. The effect of crystallite size on pressure amplification in switchable porous solids. *Nat. Commun.* **2018**, *9*, No. 1573.
(24) Krause, S.; Evans, J. D.; Bon, V.; Senkovska, I.; Iacomi, P.; Kolbe, F.; Ehrling, S.; Troschke, E.; Getzschmann, J.; Többens, D. M.; Franz, A.; Wallacher, D.; Yot, P. G.; Maurin, G.; Brunner, E.; Llewellyn, P. L.; Coudert, F.-X.; Kaskel, S. Towards general network architecture design criteria for negative gas adsorption transitions in ultraporous frameworks. *Nat. Commun.* **2019**, *10*, No. 3632.
(25) Krause, S.; Reuter, F. S.; Ehrling, S.; Bon, V.; Senkovska, I.; Kaskel, S.; Brunner, E. Impact of Defects and Crystal Size on Negative Gas Adsorption in DUT-49 Analyzed by In Situ^{129}Xe NMR Spectroscopy. *Chem. Mater.* **2020**, *32*, 4641−4650.
(26) Kolbe, F.; Krause, S.; Bon, V.; Senkovska, I.; Kaskel, S.; Brunner, E. High-Pressure in Situ ^{129} Xe NMR Spectroscopy: Insights into Switching Mechanisms of Flexible Metal−Organic Frameworks Isoreticular to DUT-49. *Chem. Mater.* **2019**, *31*, 6193−6201.
(27) Krause, S.; Evans, J. D.; Bon, V.; Senkovska, I.; Coudert, F.-X.; Többens, D. M.; Wallacher, D.; Grimm, N.; Kaskel, S. The role of temperature and adsorbate on negative gas adsorption transitions of the mesoporous metal-organic framework DUT-49. *Faraday Discuss.* **2021**, *225*, 168−183.
(28) Walenszus, F.; Bon, V.; Evans, J. D.; Kaskel, S.; Dvoyashkin, M. Molecular Diffusion in a Flexible Mesoporous Metal-Organic Framework over the Course of Structural Contraction. *J. Phys. Chem. Lett.* **2020**, *11*, 9696−9701.
(29) Bon, V.; Krause, S.; Senkovska, I.; Grimm, N.; Wallacher, D.; Többens, D. M.; Kaskel, S. Massive pressure amplification by stimulated contraction of mesoporous frameworks. *Angew. Chem., Int. Ed.* **2021**, *60*, 11735−11739.
(30) Schaber, J.; Krause, S.; Paasch, S.; Senkovska, I.; Bon, V.; Többens, D. M.; Wallacher, D.; Kaskel, S.; Brunner, E. In Situ Monitoring of Unique Switching Transitions in the Pressure-Amplifying Flexible Framework Material DUT-49 by High-Pressure ^{129}Xe NMR Spectroscopy. *J. Phys. Chem. C* **2017**, *121*, 5195−5200.
(31) Allendorf, M. D.; Bauer, C. A.; Bhakta, R. K.; Houk, R. J. T. Luminescent metal−organic frameworks. *Chem. Soc. Rev.* **2009**, *38*, 1330.
(32) Hu, Z.; Deibert, B. J.; Li, J. Luminescent metal−organic frameworks for chemical sensing and explosive detection. *Chem. Soc. Rev.* **2014**, *43*, 5815−5840.
(33) Anik, Ü.; Timur, S.; Dursun, Z. Metal organic frameworks in electrochemical and optical sensing platforms: a review. *Microchim. Acta* **2019**, *186*, No. 196.
(34) Newsome, W. J.; Chakraborty, A.; Ly, R. T.; Pour, G. S.; Fairchild, D. C.; Morris, A. J.; Uribe-Romo, F. J. J-dimer emission in interwoven metal−organic frameworks. *Chem. Sci.* **2020**, *11*, 4391−4396.
(35) Yang, L.; Song, Y.; Wang, L. Multi-emission metal−organic framework composites for multicomponent ratiometric fluorescence sensing: recent developments and future challenges. *J. Mater. Chem. B* **2020**, *8*, 3292−3315.
(36) Wei, Z.; Chen, D.; Guo, Z.; Jia, P.; Xing, H. Eosin Y-Embedded Zirconium-Based Metal−Organic Framework as a Dual-Emitting Built-In Self-Calibrating Platform for Pesticide Detection. *Inorg. Chem.* **2020**, *59*, 5386−5393.
(37) Li, X.; Yu, J.; Gosztola, D. J.; Fry, H. C.; Deria, P. Wavelength-Dependent Energy and Charge Transfer in MOF: A Step toward Artificial Porous Light-Harvesting System. *J. Am. Chem. Soc.* **2019**, *141*, 16849−16857.
(38) Cui, Y.; Yue, Y.; Qian, G.; Chen, B. Luminescent Functional Metal−Organic Frameworks. *Chem. Rev.* **2012**, *112*, 1126−1162.
(39) Sabbatini, N.; Guardigli, M.; Lehn, J.-M. Luminescent lanthanide complexes as photochemical supramolecular devices. *Coord. Chem. Rev.* **1993**, *123*, 201−228.
(40) Bannwarth, C.; Ehlert, S.; Grimme, S. GFN2-xTB—An Accurate and Broadly Parametrized Self-Consistent Tight-Binding Quantum Chemical Method with Multipole Electrostatics and Density-Dependent Dispersion Contributions. *J. Chem. Theory Comput.* **2019**, *15*, 1652−1671.
(41) Garai, B.; Bon, V.; Krause, S.; Schwotzer, F.; Gerlach, M.; Senkovska, I.; Kaskel, S. Tunable Flexibility and Porosity of the Metal−Organic Framework DUT-49 through Postsynthetic Metal Exchange. *Chem. Mater.* **2020**, *32*, 889−896.
(42) Garai, B.; Bon, V.; Walenszus, F.; Khadiev, A.; Novikov, D. V.; Kaskel, S. Elucidating the Structural Evolution of a Highly Porous Responsive Metal−Organic Framework (DUT-49(M)) upon Guest Desorption by Time-Resolved in Situ Powder X-ray Diffraction. *Cryst. Growth Des.* **2021**, *21*, 270−276.